Two-Dimensional Finite Element Analysis of Microwave Heating

K. G. Ayappa and H. T. Davis
Dept. of Chemical Engineering and Materials Science, University of Minnesota, Minneapolis, MN 55455

E. A. Davis and J. Gordon
Dept. of Food Science and Nutrition, University of Minnesota, St. Paul, MN 55108

Transient temperature profiles for long rods of lossy dielectric materials with thermally-dependent dielectric properties exposed to uniform plane waves are obtained. Maxwell's equations and the heat equation are simultaneously solved using the finite element method to predict the power absorbed and the resulting temperature rise in samples of square and circular cross-section. Following the method introduced recently, we derive an exact radiation boundary condition which is independent of the rod cross-section. For a cylindrical sample, the boundary condition is imposed on the cylinder itself. For a square rod, the boundary condition is imposed on a cylinder containing the rod. The temperature dependence of dielectric properties and sample dimensions appreciably influence heating patterns. For square samples, the edges focus radiation, causing preferential heating at the edges. This effect is pronounced for larger samples. In addition, the incident wave polarization influences the heating of the rod. For waves where the electric field is polarized along the long axis of the sample (TM^z polarization) the power absorbed is higher than when the electric field is perpendicular to the axis (TE^z polarization). A case involving runaway heating is also investigated.

Introduction

The use of microwaves as a source of thermal energy is rapidly growing. The food industry is the largest consumer of microwave energy. Microwaves are used in ceramic processing for drying and sintering (Chabinsky, 1988) and in the polymer industry to cure epoxy resins (Jow et al., 1988; Le Van et al., 1987). It is also employed in the drying of paper, forest products and textiles (Chabinsky, 1988).

As a result of dielectric losses, microwave absorption provides a volumetrically-distributed heat source. The temperature distribution in a substance subjected to microwave radiation is thus governed by the interaction and absorption of radiation by the medium and the accompanying transport processes due to the dissipation of electrical energy into heat. To model transient temperature distributions the absorbed microwave power is deduced by solving Maxwell's equations and is incorporated as a source term in the transient heat equation. If the material's thermal and dielectric properties are constant, the problem is linear and Maxwell's equations can be solved independent of the heat equation. Scattering and absorption of plane electromagnetic waves by 2- and 3-D objects with constant dielectric properties have received considerable attention. Scattering is concerned with the field distribution external to the sample, and absorption is concerned with the field within the object. However, most analysis of scattering involves deducing the field distribution within the object as well. In either case, computing electric fields involves solving Maxwell's equations in an unbounded domain. The techniques can be broadly classified into methods using either an integral or differential formulation of Maxwell's equations (Speigel, 1984). The integral equation formulations are popular, since the behavior of the far field is built into the formulation (Richmond,

Correspondence concerning this article should be addressed to H. T. Davis.

1964). Integral formulations, however, result in dense matrices. In the differential formulations, considerable attention has been given to the manner in which the domain around the sample is truncated and the nature of the boundary condition imposed. These boundary conditions are commonly referred to as either absorbing or radiation boundary conditions (RBC) and are imposed on a synthetic boundary surrounding the sample. Differential forms of Maxwell's equations are solved either in the time or in the frequency domain. In the latter method, the time derivatives are eliminated by assuming that the field variables have a frequency dependence of either $e^{i\omega t}$ or $e^{-i\omega t}$ (Balanis, 1989).

RBCs have been discussed by Keller and Givoli (1989), Mittra et al. (1989), D'Angelo and Mayergoyz (1989), and Blaschak and Kriegsmann (1988). The boundary condition derived by Keller and Givoli (1989) is exact, but global in nature, as it involves evaluating an integral over the boundary of the sample. They have indicated the accuracy of the exact RBC by comparing it with other approximate local RBCs. The primary advantage of the exact RBC is that the accuracy of the solution does not depend on the proximity of the synthetic boundary to the sample. A similar approach has been used by Pearson et al. (1989) to derive an exact RBC. Here, the RBC is compared to the approximate Bayliss and Turkel RBC, and the latter is seen to perform to within 3% of the exact RBC. Marin (1982) derives an exact global RBC which involves solving an integral equation on the synthetic boundary.

Analytic formulations for the scattering of plane waves from dielectric cylinders have been studied by Bussey and Richmond (1975) and Chang and Mei (1976). A finite element formulation for scattering from inhomogeneous dielectric cylinders was developed by Peterson and Castillo (1989) where the approximate radiation condition developed by Bayliss and Turkel (1980) is employed. Britt (1989) uses a finite difference time domain analysis, while Cangellaris (1987) uses a time domain finite element formulation for scattering in 2D. Frequency domain analysis for electromagnetic scattering has been reviewed by Glisson (1989).

Absorption of electromagnetic energy in multilayered cylinders was studied analytically by Massoudi et al. (1979) and Ruppin (1979). Analytic electric field distributions in cylinders of finite length exposed to an aperture source have been obtained by Wait (1987). Lynch et al. (1985) and Lee and Madsen (1990) use frequency and time domain methods to deduce electric field intensities with finite elements in 2-D objects with a uniform electric field (Dirichlet boundary condition) at the boundary. Using a hybrid finite element/boundary element method, Lynch et al. (1986) and Paulsen et al. (1986) obtained electric field distributions in lossy dielectrics to investigate heat effects of cancer therapy. Finite difference time domain methods to determine field distributions have been used by Yee (1966), Taflove (1980), Taflove and Brodwin (1975), and Dennis et al. (1987, 1988). An integral equation approach for electromagnetic fields induced inside arbitrarily shaped bodies has been studied by Livesay and Chen (1974). Time domain finite difference solutions for 2-D absorption have been compared with integral equation formulations by Borup et al. (1987).

Analysis of microwave heating in materials with constant material properties by solving the heat conduction equation with the microwave energy deduced from Maxwell's equations has been used by Nachman and Turgeon (1984) and Taflove and Brodwin (1975). The former investigate temperature patterns in multilayered media on a reflecting support, and in the latter temperature distributions in the human eye are obtained.

Dielectric properties of most materials vary with temperature. As a consequence, the deposition of microwave energy is a function of the spatially varying dielectric constant in the medium. Temperature dependence of the properties results in a coupled nonlinear problem, and so Maxwell's equations must be solved simultaneously with the heat equation to predict the thermal response of the object. Foods at frequencies between 400–900 MHz show strong temperature-sensitive dielectric behavior, but the variation is less pronounced at 2,800 MHz (Ohlsson and Bengtsson, 1975). During drying, dielectric properties vary spatially within the sample primarily due to the variation in moisture content (Wei et al., 1985). Changes in dielectric properties alter the penetration of radiation during heating, and a sharp increase in the dielectric loss with temperature can lead to runaway conditions (Ayappa et al., 1991). Microwave heating in 1D using Maxwell's equations to determine the power absorption in materials with temperature-dependent properties has been modeled by De Wagter (1984), Ayappa et al. (1991), Jolly and Turner (1990), and Smyth (1990).

The electromagnetics literature on 2- and 3-D models focuses on the scattered and/or the absorbed microwave field for materials with constant dielectric properties. In microwave heating applications, in addition to the absorbed field, the resulting temperature distribution is of interest. Sample geometry and size influence the amount of adsorbed power and alter the heating. Edges and corners are known to focus power and heat up rapidly. Risman et al. (1987) have observed pronounced edge heating in experiments conducted in domestic microwave ovens. Microwave power was observed to concentrate 1 to 2 cm from the incident face and around the top periphery of the sample. The phenomenon was observed for any large sample size. In addition to the frequency of radiation and thermal dependence of material properties, the polarization of the incident radiation or equivalently the orientation of the sample effects the absorbed power (Gandhi, 1975). These effects are important when designing products to be processed with microwaves and can be studied in models of microwave heating in 2 and 3 dimensions.

To understand these various effects on the heating of samples by microwaves, we have developed a 2-D finite element model to predict the temperature rise in rod-like samples exposed to a plane wave. The power absorbed by the object and temperature distributions are obtained by simultaneously solving Maxwell's equations in the frequency domain with the transient heat equation. Dielectric properties are assumed to be temperature-dependent, and the heating of rods with circular and square cross-section are compared. Influence of the sample size and incident wave polarizations on absorbed power and temperature patterns are illustrated. The incident wave is TM^z-polarized when the electric field is polarized along the axis of the rod and TE^z when the electric field is perpendicular to the axis. The exact RBC as derived by Keller and Givoli is extended to incorporate the incident field. For cylindrical samples, this boundary condition is imposed on the surface of the cylinder; for the square rod, the synthetic boundary is a cylinder enclosing the object.

Wave Propagation

The basic equations governing the electric and magnetic field vectors in the sample are derived from the Maxwell curl relations and the governing equations, and boundary conditions for the two different polarizations are discussed. A propagating electromagnetic wave is composed of oscillating electric (E) and magnetic (H) field components. Maxwell's equations describing their space and time dependence are (in rationalized mks units):

$$\nabla \times E = -\frac{\partial B}{\partial t} \quad \text{and} \quad \nabla \times H = J + \frac{\partial D}{\partial t}, \tag{1}$$

where E and H are the electric and magnetic fields, J the current flux, D electric displacement, and B magnetic induction. The constitutive relations relating J, D and B to E and H are:

$$J = \sigma(\omega)E(t) \quad D = \epsilon(\omega)E(T) \text{ and } B = \mu(\omega)H(t), \tag{2}$$

where $E = \overline{E}e^{-i\omega t}$ and $H = \overline{H}e^{-i\omega t}$. Alternatively $e^{j\omega t}$ can be used to express the time dependence. Equations 1 and 2 yield:

$$\nabla \times \overline{E} = i\omega\mu(\omega)\overline{H} \tag{3}$$

and

$$\nabla \times \overline{H} = [\sigma(\omega) - i\omega\epsilon(\omega)]\overline{E} \equiv -i\omega\epsilon^*\overline{E}. \tag{4}$$

where the "complex dielectric constant" ϵ^* is defined as:

$$\epsilon^*(\omega) \equiv \epsilon(\omega) + \frac{i\sigma(\omega)}{\omega} \equiv \epsilon'(\omega) + i\epsilon''(\omega). \tag{5}$$

The materials ability to store electrical energy is represented by $\epsilon' = Re(\epsilon^*)$, and $\epsilon'' = Im(\epsilon^*)$ accounts for losses through energy dissipation. The conductivity, $\sigma(\omega)$, dielectric constant, $\epsilon(\omega)$, and magnetic permeability, $\mu(\omega)$, are complex functions of the frequency ω of the radiation. These individual contributions must be measured or predicted by a suitable theory. For most materials used in microwave heating applications, the magnetic permeability $\mu(\omega)$ is well approximated by its value μ_0 in free space. In what follows, we assume this to be true. Taking the divergence of Eqs. 3 and 4, the relations

$$\nabla \cdot (\epsilon^*\overline{E}) = 0 \quad \text{and} \quad \nabla \cdot (\mu\overline{H}) = 0 \tag{6}$$

are obtained. The material properties are temperature-dependent, and so σ and ϵ in Eq. 2 are implicit functions of time. Since the time scale of electromagnetic propagation is significantly smaller than the time scales for thermal diffusion, an order of magnitude analysis indicates that the terms involving the time derivatives of σ and ϵ are very small and can be neglected. With this assumption, and the condition of electroneutrality of the materials considered [which implies $\nabla \cdot (\epsilon^*\overline{E}) = 0$], Eqs. 3 and 4 can be combined to find:

$$\nabla\left(\overline{E} \cdot \frac{\nabla\epsilon^*}{\epsilon^*}\right) + \nabla^2\overline{E} + k^2\overline{E} = 0, \tag{7}$$

where

$$k^2 = \frac{\omega^2}{c^2}(\kappa' + i\kappa''). \tag{8}$$

The relative dielectric constant κ' and the relative dielectric loss κ'', are:

$$\kappa' \equiv \epsilon'/\epsilon_0 \quad \text{and} \quad \kappa'' \equiv \epsilon''/\epsilon_0, \tag{9}$$

and $c = 1/\sqrt{\mu_0\epsilon_0}$ where c is the speed of light. To derive an equation for the magnetic field H, Eqs. 3 and 4 can be combined to find:

$$\nabla^2\overline{H} + k^2\overline{H} - i\omega\nabla\epsilon^* \times \overline{E} = 0. \tag{10}$$

The last term in the lefthand side of Eq. 10 is due to the spatial variation of ϵ^* because of the temperature dependence of the dielectric properties. To simplify notation, the overbar on $\overline{E}$ and $\overline{H}$ will be dropped from this point on. The propagation constant k can be represented as a complex quantity:

$$k = \alpha + i\beta, \tag{11}$$

where α and β are related to the dielectric properties of the medium and frequency of radiation by:

$$\alpha = \frac{2\pi f}{c}\sqrt{\frac{\kappa'(\sqrt{1+\tan^2\delta}+1)}{2}} \tag{12}$$

and

$$\beta = \frac{2\pi f}{c}\sqrt{\frac{\kappa'(\sqrt{1+\tan^2\delta}-1)}{2}} \tag{13}$$

where

$$\tan\delta = \frac{\kappa''}{\kappa'}. \tag{14}$$

In Eqs. 12 and 13 we have replaced ω by $2\pi f$, where f is the frequency of radiation. The phase constant α represents the change of phase of the propagating wave and is related to the wavelength of radiation in the medium (λ_m) by:

$$\lambda_m = \frac{2\pi}{\alpha}, \tag{15}$$

which in free space reduces to $\lambda_0 = c/f$. The attenuation constant β controls the rate at which the incident field intensity E_0 decays into a sample. For instance, in a semi-infinite sample the interior field obeys the equation:

$$E = E_0 e^{-\beta z}. \tag{16}$$

Thus, for higher frequencies, β increases and the penetration of microwaves into the sample decreases. The quantity β^{-1} is known as the characteristic penetration depth, that is, the

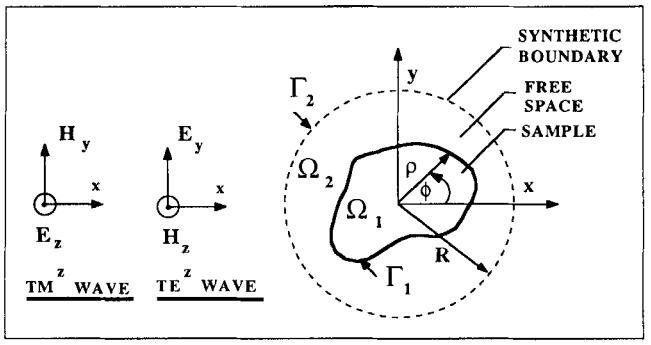

Figure 1. Sample exposed to plane waves.

distance at which the field intensity decreases to $1/e$ of its incident value. With a knowledge of the electric field distribution in the medium the local power dissipated in the medium is:

$$p(r)=\frac{1}{2}\,\omega\epsilon_0\kappa''\boldsymbol{E}\cdot\boldsymbol{E}^*, \tag{17}$$

where $\boldsymbol{E}^*$ is the complex conjugate of $\boldsymbol{E}$.

The boundary conditions relating the electric and magnetic components at the interface between two media 1 and 2 for a lossy dielectric are:

$$\boldsymbol{n}\cdot(\epsilon_1^*\boldsymbol{E}_1-\epsilon_2^*\boldsymbol{E}_2)=0 \tag{18a}$$

$$\boldsymbol{n}\times(\boldsymbol{E}_1-\boldsymbol{E}_2)=0 \tag{18b}$$

$$\boldsymbol{n}\cdot(\mu_1\boldsymbol{H}_1-\mu_2\boldsymbol{H}_2)=0 \tag{18c}$$

$$\boldsymbol{n}\times(\boldsymbol{H}_1-\boldsymbol{H}_2)=0 \tag{18d}$$

where $\boldsymbol{n}$ is the unit outward normal. These boundary conditions assume that there are no sources, that is, charges at the interface between the two medium. Equations 18a and 18c imply that the normal components of the electric and magnetic fields are discontinuous across the interface. Equations 18b and 18d indicate that the tangential components are continuous across the interface.

TM^z polarization

Consider the rod with arbitrary cross-section shown in Figure 1. Here, the electric field of the incident wave is polarized along the long axis of the rod. A cylinder of radius R encloses the sample and is denoted by Γ_2. The region Ω_2 bounded by the surfaces Γ_1 and Γ_2 denotes free space. If Ω_1 denotes the sample, then $\Omega=\Omega_1+\Omega_2$ is the entire domain. Since the sample is infinite in the z direction, for the (TE^z) case the field component E_z varies in the $r-\phi$ plane only. Equation 7 for the electric field in Ω is:

$$\nabla^2 E_{z,l}+k_l^2 E_{z,l}=0, \tag{19}$$

where

$$k_l^2=\frac{\omega^2}{c^2}\,(\kappa_l'+i\kappa_l'') \quad \text{and} \quad l=1,2.$$

The boundary conditions (Eqs. 18b and 18d) imply that the z components of the electric field E_z and the ϕ components of the magnetic field (H_ϕ) are continuous. Using Eq. 3 to relate H_ϕ to E_z, these boundary conditions are:

$$\left.\begin{aligned} E_{z,1}&=E_{z,2}\\ \frac{\partial E_{z,1}}{\partial\rho}&=\frac{\partial E_{z,2}}{\partial\rho}\end{aligned}\right\} \quad \text{on} \quad \Gamma_1. \tag{20}$$

A radiation boundary condition is used on Γ_2 and will be derived later. Using the dimensionless variables:

$$r=\frac{\rho}{R}, \quad E_{z,l}^*=\frac{E_{z,l}}{E_0}, \quad \nabla^*=R\nabla \tag{21}$$

Equation 19 reduces to:

$$\nabla^{*2}E_{z,l}^*+k_l^{*2}E_{z,l}^*=0, \tag{22}$$

where

$$k_l^*=Rk_l. \tag{23}$$

If $E_{z,l}^*=E_{z,l}^R+iE_{z,l}^I$, then equating the real and imaginary components of Eq. 19 we get:

$$\nabla^{*2}E_{z,l}^R+E_{z,l}^R\psi_l^E-E_{z,l}^I\chi_l^E=0 \tag{24}$$

and

$$\nabla^{*2}E_{z,l}^I+E_{z,l}^I\psi_l^E+E_{z,l}^R\chi_l^E=0 \tag{25}$$

where $\psi_l^E=R^2\omega^2\kappa_l'/c^2$ and $\chi_l^E=R^2\omega^2\kappa_l''/c^2$. The boundary condition (Eq. 20) for the real and imaginary components are:

$$\left.\begin{aligned} E_{z,1}^L&=E_{z,2}^L\\ \frac{\partial E_{z,1}^L}{\partial r}&=\frac{\partial E_{z,2}^L}{\partial r}\end{aligned}\right\} \quad \text{for} \quad L=R,I \tag{26}$$

The power absorbed by the sample from Eq. 17 is:

$$p_1(r,\phi)=\frac{1}{2}\,\omega\epsilon_0\kappa''E_0^2[E_{z,1}^{R\,2}+E_{z,1}^{I\,2}] \tag{27}$$

TE^z polarization

Here the magnetic field is oriented along the long axis of the rod. For the TE^z the electric field vector has two components, E_ρ and E_ϕ, in the sample. However, the magnetic field has only the $H_z(\rho,\phi)$ component. Hence, it is simpler to solve for the magnetic field and deduce the electric field components using Eq. 4. Since material properties vary only in the $\rho-\phi$ plane and the electric field has no z component, Eqs. 3 and 4 can be combined to find:

$$\nabla \cdot \frac{1}{\kappa_l^*} \nabla H_{z,l} + k_0^2 H_{z,l} = 0, \tag{28}$$

for

$$l = 1,2$$

where $k_0^2 = \omega^2/c^2$, and $\kappa_l^* = \kappa_l' + i\kappa_l''$. The form of Eq. 28 for the magnetic field is useful since boundary conditions can be conveniently incorporated during the finite element analysis. The boundary conditions from Eqs. 18 imply that the z component of the magnetic field and the ϕ components of the electric field are continuous across the interface. Using Eq. 4 to relate the ϕ component of the electric field to the magnetic field, the boundary conditions are:

$$\left.\begin{aligned} H_{z,1} &= H_{z,2} \\ \frac{\partial H_{z,1}}{\epsilon_1^* \partial \rho} &= \frac{\partial H_{z,2}}{\epsilon_2^* \partial \rho} \end{aligned}\right\} \quad \text{on} \quad \Gamma_1 \tag{29}$$

The RBC on Γ_2 is similar to the RBC for the TE^z case which will be derived later. The solution to the magnetic field is obtained in an identical manner as the solution to the electric field for the TM^z wave. Once the solution to H_z is obtained the electric field components determined from Eq. 4 are:

$$E_{\phi,l} = \frac{1}{i\omega\epsilon_l^*} \frac{\partial H_{z,l}}{\partial \rho} \tag{30}$$

and

$$E_{\rho,l} = \frac{-1}{i\rho\omega\epsilon_l^*} \frac{\partial H_{z,l}}{\partial \phi} \tag{31}$$

If

$$H_{z,l}^* = \frac{H_{z,l}}{H_0}, \quad E_{\phi,l}^* = \frac{E_{\phi,l}}{E_0}, \quad E_{\rho,l}^* = \frac{E_{\rho,l}}{E_0}$$

and $H_{z,l}^* = H_{z,l}^R + iH_{z,l}^I$, then equating the real and imaginary components of Eq. 28 in dimensionless form:

$$\nabla^* \cdot \psi_l^H \nabla^* H_{z,l}^R + \nabla^* \cdot \chi_l^H \nabla^* H_{z,l}^I + k_0^{*2} H_{z,l}^R = 0 \tag{32}$$

and

$$\nabla^* \cdot \psi_l^H \nabla^* H_{z,l}^I - \nabla^* \cdot \chi_l^H \nabla^* H_{z,l}^R + k_0^{*2} H_{z,l}^I = 0 \tag{33}$$

where

$$\psi_l^H = \frac{\kappa_l'}{\kappa_l'^2 + \kappa_l''^2}, \quad \chi_l^H = \frac{\kappa_l''}{\kappa_l'^2 + \kappa_l''^2} \quad \text{and} \quad k_0^* = Rk_0.$$

Equating the real and imaginary components of Eq. 29, the boundary conditions in dimensionless form are:

$$\left.\begin{aligned} \frac{\partial H_{z,2}^I}{\partial r} &= \psi_1^H \frac{\partial H_{z,1}^R}{\partial r} + \chi_1^H \frac{\partial H_{z,1}^I}{\partial r} \quad \text{and} \quad H_{z,2}^R = H_{z,1}^R \\ \frac{\partial H_{z,2}^R}{\partial r} &= \psi_1^H \frac{\partial H_{z,1}^I}{\partial r} - \chi_1^H \frac{\partial H_{z,1}^R}{\partial r} \quad \text{and} \quad H_{z,2}^I = H_{z,1}^I \end{aligned}\right\} \quad \text{on} \quad \Gamma_1. \tag{34}$$

Equations 30 and 31 in dimensionless form are:

$$E_{\phi,l}^* = \frac{1}{k_0^* \kappa_l^*} \left[\frac{\partial H_{z,l}^I}{\partial r} - i \frac{\partial H_{z,l}^R}{\partial r} \right] \tag{35}$$

and

$$E_{\rho,l}^* = \frac{-1}{k_0^* \kappa_l^* r} \left[\frac{\partial H_{z,l}^I}{\partial \phi} - i \frac{\partial H_{z,l}^R}{\partial \phi} \right], \tag{36}$$

where $E_0/H_0 = \sqrt{\mu_0/\epsilon_0}$ the free space wave impedance has been used. The power absorbed by the sample, medium 1, from Eq. 17 for the TE^z case is:

$$p_1(r,\phi) = \frac{\omega\epsilon_0 E_0^2 \chi_1^H}{2k_0^{*2}} \left[\left(\frac{\partial H_{z,1}^I}{\partial r} \right)^2 + \left(\frac{\partial H_{z,1}^R}{\partial r} \right)^2 + \left(\frac{1}{r} \frac{\partial H_{z,1}^I}{\partial \phi} \right)^2 + \left(\frac{1}{r} \frac{\partial H_{z,1}^R}{\partial \phi} \right)^2 \right] \tag{37}$$

Radiation boundary condition

For a given incident plane wave on the sample some of the radiation is scattered and the rest absorbed. As mentioned earlier, the domain of such problems is unbounded and many methods have been devised to impose boundary conditions that minimize the domain of analysis. With regard to microwave heating, the absorbed field is of primary interest, and one seeks to minimize modeling the space around the sample. Perhaps the best formulation in this regard is the exact RBC developed by Keller and Givoli (1989) to study scattered field patterns. This boundary condition is imposed on the surface of the cylinder for samples with circular cross-section, and for other shapes the boundary condition is imposed on a cylindrical surface enclosing the sample. Further, this cylindrical surface can be placed as close to the sample as desired. Another advantage of the RBC is the ease in which it can be incorporated into the finite element analysis. Here, the RBC is developed to include the incident field and is imposed on a cylindrical surface of radius R surrounding the object. The RBC is presented here for the TM^z polarization. The derivation for the TE^z polarization is similar, except that the electric field is replaced by the magnetic field. To facilitate the derivation of the RBC in free space the incident plane wave is represented in $\rho - \phi$ co-ordinates by means of a cylindrical wave transformation (Balanis, 1989). For a $e^{-i\omega t}$ time dependence the incident wave traveling in the x direction is:

$$E_{z,2}^{(i)} = \sum_{n=-\infty}^{\infty} E_0 i^n J_n(k_2\rho) e^{in\phi} \tag{38}$$

where $J_n(x)$ is the nth-order Bessel function of the first kind, and k_2 is the propagation constant in medium 2 (free space in our case). The outgoing scattered wave $E_{z,2}^{(s)}$ is:

$$E_{z,2}^{(s)} = \sum_{n=-\infty}^{\infty} E_0 b_n H_n^{(1)}(k_2\rho) e^{in\phi} \tag{39}$$

where $H_n^{(1)}(x) = J_n(x) + iY_n(x)$ is the Hankel function of the

first kind, and Y_n is the nth-order Bessel function of the second kind (Abramowitz and Stegun, 1970). The total electric field E_z exterior to the sample is obtained by superimposing the incident and scattered waves:

$$E_{z,2}(\rho,\phi)=E_{z,2}^{(i)}+E_{z,2}^{(s)} \tag{40}$$

Equation 40 written in dimensionless form is:

$$E_{z,2}^{*}=\sum_{n=-\infty}^{\infty} i^n J_n(k_2^{*}r)e^{in\phi}+\sum_{n=-\infty}^{\infty} b_n H_n^{(1)}(k_2^{*}r)e^{in\phi}, \tag{41}$$

where $k_2^{*}=k_2R$. The coefficients b_n are determined by evaluating $E_{z,2}^{*}(r,\phi)$ at $r=1$ and using the orthogonality of the eigenfunctions $e^{in\phi}$:

$$\int_0^{\infty} e^{i(n-m)\phi}d\phi=\begin{cases}2\pi, & n=m;\\ =0, & n\neq m.\end{cases} \tag{42}$$

The RBC obtained at $r=1$, by taking the derivative of $E_{z,2}^{*}$ with respect to r is:

$$\frac{\partial E_{z,2}^{*}}{\partial r}=\sum_{n=0}^{\infty}C_n\cos n\phi + \sum_{n=0}^{\infty}D_n\int_0^{2\pi}E_{z,2}^{*}(1,\phi')\cos n(\phi-\phi')d\phi' \tag{43}$$

where the coefficients

$$C_n=\epsilon_n i^n k_2^{*}\left[J_n'(k_2^{*})-J_n(k_2^{*})\frac{H_n^{(1)\prime}(k_2^{*})}{H_n^{(1)}(k_2^{*})}\right]$$

and

$$D_n=\frac{\delta_n k_2^{*}H_n^{(1)\prime}(k_2^{*})}{\pi H_n^{(1)}(k_2^{*})}, \tag{44}$$

and

$$\epsilon_n=\begin{cases}1, & n=0;\\ =2, & \text{otherwise,}\end{cases}\quad\text{and}\quad \delta_n=\begin{cases}1/2, & n=0;\\ =1, & \text{otherwise.}\end{cases} \tag{45}$$

The prime indicates differentiation w.r.t. the argument of the special functions, and so

$$J_n'(k_2^{*})=-J_{n+1}(k_2^{*})+(n/k_2^{*})J_n(k_2^{*}); \tag{46}$$

and

$$H_n^{(1)\prime}(k_2^{*})=-J_{n+1}(k_2^{*})+(n/k_2^{*})J_n(k_2^{*}) + i[-Y_{n+1}(k_2^{*})+(n/k_2^{*})Y_n(k_2^{*})]. \tag{47}$$

If the incident field is absent, Eq. 43 reduces to the form as derived by Keller and Givoli (1989). Since, $E_{z,2}^{*}=E_{z,2}^{R}+iE_{z,2}^{I}$, then equating the real and imaginary parts of Eq. 43 the boundary condition at $r=1$ is:

$$\frac{\partial E_{z,2}^{R}}{\partial r}=\sum_{n=0}^{\infty}Re(C_n)\cos n\phi + \sum_{n=0}^{\infty}Re(D_n)\int_0^{2\pi}E_{z,2}^{R}(1,\phi')\cos n(\phi-\phi')d\phi' - \sum_{n=0}^{\infty}Im(D_n)\int_0^{2\pi}E_{z,2}^{I}(1,\phi')\cos n(\phi-\phi')d\phi' \tag{48}$$

and

$$\frac{\partial E_{z,2}^{I}}{\partial r}=\sum_{n=0}^{\infty}Im(C_n)\cos n\phi + \sum_{n=0}^{\infty}Im(D_n)\int_0^{2\pi}E_{z,2}^{R}(1,\phi')\cos n(\phi-\phi')d\phi' + \sum_{n=0}^{\infty}Re(D_n)\int_0^{2\pi}E_{z,2}^{I}(1,\phi')\cos n(\phi-\phi')d\phi' \tag{49}$$

Heat Equation

The temperature of the sample exposed to radiation is determined by solving the heat conduction equation with the microwave power included as a heat source term. The sample is assumed to be homogeneous and isotropic, and moisture loss is neglected. The time-dependent energy equation governing the temperature distribution in the region Ω_1 is:

$$\rho C_p\frac{\partial T}{\partial t}=\nabla\cdot(k\nabla T)+p(r,T), \tag{50}$$

where ρ, C_p, and k are the material density, specific heat capacity, and thermal conductivity, respectively. The microwave power, which is a function of the electric field distribution, depends on temperature due to the variation of dielectric properties with temperature. At the boundaries of the sample, Γ_1 heat is lost to the surroundings by convection. The boundary condition here is:

$$-\boldsymbol{n}\cdot k\nabla T=h(T-T_\infty) \tag{51}$$

where $\boldsymbol{n}$ is the outward pointing unit normal on Γ_1, T_∞ is the ambient temperature, and h is the heat-transfer coefficient. If ρ_0, C_{p0} and k_0 are reference thermal properties, then dividing Eq. 50 by k_0 and using the dimensionless variables:

$$r=\frac{\rho}{R},\quad \theta=\frac{T-T_\infty}{T_0},$$

$$Bi=\frac{hR}{k_0},\quad \tau=\frac{\alpha_0 t}{R^2},$$

the transient heat conduction equation is:

$$\overline{\rho C_p}\frac{\partial\theta}{\partial\tau}=\nabla^{*}\cdot(\bar{k}\nabla^{*}\theta)+P(r,\phi,\theta), \tag{52}$$

where

$$P=\frac{pR^2}{k_0T_0},\quad \overline{\rho C_p}=\frac{\rho C_p}{\rho_0 C_{p,0}}\quad\text{and}\quad \bar{k}=\frac{k}{k_0}.$$

The boundary condition is:

$$-\boldsymbol{n}\cdot\bar{k}\nabla^*\theta=Bi\theta, \tag{53}$$

and the initial condition is:

$$\theta(\tau=0)=0\quad\text{in}\quad\Omega_1. \tag{54}$$

Exact Solutions for Electric Field

Solutions for the electric field intensities in cylindrical samples with constant properties are well known and are given below for both polarizations considered. The derivations are along the lines of the scattered field formulations for pure conductors given in Balanis (1989). The solutions are obtained by expanding the field both externally and internally in Bessel functions and deducing the expansion coefficients with appropriate boundary and interface conditions.

Electric field for TM^z polarization

Using the dimensionless variables:

$$E^*_{z,l}=\frac{E_{z,l}}{E_0},\quad r=\frac{\rho}{R}\quad\text{and}\quad k_l^*=k_lR$$

the electric field external to the sample in medium 2, free space, which is a linear combination of incident and scattered fields is:

$$E^*_{z,2}(r,\phi)=\sum_{n=0}^{\infty}[\epsilon_n i^n J_n(k_2^*r)+b_nH_n^{(1)}(k_2^*r)]\cos n\phi, \tag{55}$$

where

$$\epsilon_n=\begin{cases}1, & n=0;\\ =2, & \text{otherwise.}\end{cases}$$

The field induced in the cylinder, medium 1 is:

$$E^*_{z,1}=\sum_{n=0}^{\infty}c_nJ_n(k_1^*r)\cos n\phi. \tag{56}$$

The boundary conditions at $r=1$ are given by Eq. 20. Incorporating the boundary conditions and equating coefficients in the expansions:

$$c_n=\epsilon_n i^n\left[\frac{J_n'(k_2^*)H_n^{(1)}(k_2^*)-J_n(k_2^*)H_n^{(1)'}(k_2^*)}{\sqrt{\kappa_1^*}J_n'(k_1^*)H_n^{(1)}(k_2^*)-J_n(k_1^*)H_n^{(1)'}(k_2^*)}\right]. \tag{57}$$

Electric field for TE^z polarization

The solution for the *TE*^{z} polarized wave consists of first obtaining the solution for the magnetic field in the sample. The electric field distribution is then deduced from Eqs. 35 and 36. Using the dimensionless variables:

$$H^*_{z,l}=\frac{H_{z,l}}{H_0},\quad r=\frac{\rho}{R}\quad\text{and}\quad k_l^*=k_lR$$

the magnetic field external to the sample in medium 2, free space, which is a linear combination of incident and scattered fields is:

$$H^*_{z,2}(r,\phi)=\sum_{n=0}^{\infty}[\epsilon_n i^n J_n(k_2^*r)+b_nH_n^{(1)}(k_2^*r)]\cos n\phi, \tag{58}$$

where

$$\epsilon_n=\begin{cases}1, & n=0;\\ =2, & \text{otherwise.}\end{cases}$$

The field induced in the cylinder, medium 1 is:

$$H^*_{z,1}=\sum_{n=0}^{\infty}c_nJ_n(k_1^*r)\cos n\phi. \tag{59}$$

The boundary conditions at $r=1$ are given by Eq. 29. Incorporating the boundary conditions and equating coefficients in the expansions:

$$c_n=\epsilon_n i^n\left[\frac{J_n'(k_2^*)H_n^{(1)}(k_2^*)-J_n(k_2^*)H_n^{(1)'}(k_2^*)}{\sqrt{1/\kappa_1^*}J_n'(k_1^*)H_n^{(1)}(k_2^*)-J_n(k_1^*)H_n^{(1)'}(k_2^*)}\right]. \tag{60}$$

With a knowledge of the magnetic field the electric field components are deduced from:

$$E^*_{\phi,1}=\frac{1}{ik_0^*\kappa_1^*}\frac{\partial H^*_{z,l}}{\partial r} \tag{61}$$

and

$$E^*_{r,l}=\frac{-1}{ik_0^*\kappa_1^*r}\frac{\partial H^*_{z,l}}{\partial\phi}. \tag{62}$$

Once the electric field distribution is known, the power is deduced from Eq. 17 and the complex algebra is conveniently performed on the computer. Bessel functions were computed using the IMSL Special Functions library routines.

Finite Element Analysis

To deduce the transient temperature profiles in the samples exposed to plane waves the field and heat equations are discretized using the Galerkin finite element method, and the resulting algebraic equations are solved using Newton's methods. The Galerkin finite element method consists of expanding the unknown, u, in a finite element basis set $\{\Phi\}$. Thus,

$$u\approx\hat{u}=\sum_{j=1}^{N}y_j\Phi^j(r). \tag{63}$$

The error or residual, $L\tilde{u}-f$, is set orthogonal to the basis functions, that is

$$\int_{\Omega}(L\tilde{u}-f)\Phi^i d\Omega=0, \tag{64}$$

for

$$i=1,\ldots,N.$$

Integrating by parts, and incorporating boundary and interface conditions, we obtain from Eq. 64 a set of differential algebraic equations whose solution yields the unknown coefficients y_j of the expansion.

Residual equations: TM^z polarization

Expanding the real ($E^R_{z,l}$) and imaginary components ($E^I_{z,l}$) of the electric field, and the temperature (θ) in the basis Φ,

$$\tilde{E}^R_{z,l}=\sum_{k=1}^{N}E^R_{z,k}\Phi^k(r),\quad \tilde{E}^I_{z,l}=\sum_{k=1}^{N}E^I_{z,k}\Phi^k(r)$$

and

$$\tilde{\theta}=\sum_{k=1}^{N}\theta_k(\tau)\Phi^k(r) \tag{65}$$

the Galerkin finite element method yields the following residual equations for Eqs. 24, 25 and 52, respectively.

$$\begin{aligned}R_i^{(1)}=&\sum_k^N E^{R,\,t+1}_{z,k}\int_{\Omega}\left[\frac{\partial\Phi^i}{\partial r}\frac{\partial\Phi^k}{\partial r}+\frac{1}{r^2}\frac{\partial\Phi^i}{\partial r}\frac{\partial\Phi^k}{\partial r}\right]rdrd\phi\\&+\sum_k E^{I,\,t+1}_{z,k}\int_{\Omega}\chi^E_l(\theta^{t+1})\Phi^i\Phi^k rdrd\phi\\&-\sum_k E^{R,\,t+1}_{z,k}\int_{\Omega}\psi^E_l(\theta^{t+1})\Phi^i\Phi^k rdrd\phi-\int_{\Gamma_2}\Phi^i\frac{\partial E^{R,\,t+1}_{z,2}}{\partial r}d\Gamma\end{aligned} \tag{66}$$

$$\begin{aligned}R_i^{(2)}=&\sum_k E^{I,\,t+1}_{z,k}\int_{\Omega}\left[\frac{\partial\Phi^i}{\partial r}\frac{\partial\Phi^k}{\partial r}+\frac{1}{r^2}\frac{\partial\Phi^i}{\partial r}\frac{\partial\Phi^k}{\partial r}\right]rdrd\phi\\&-\sum_k E^{R,\,t+1}_{z,k}\int_{\Omega}\chi^E_l(\theta^{t+1})\Phi^i\Phi^k rdrd\phi\\&-\sum_k E^{I,\,t+1}_{z,k}\int_{\Omega}\psi^E_l(\theta^{t+1})\Phi^i\Phi^k rdrd\phi-\int_{\Gamma_2}\Phi^i\frac{\partial E^{I,\,t+1}_{z,2}}{\partial r}d\Gamma\end{aligned} \tag{67}$$

$$\begin{aligned}R_i^{(3)}=&\sum_k\int_{\Omega_1}\overline{\rho C_p}\left\{\frac{\theta^{t+1}_k-\theta^t_k}{\Delta\tau}\right\}\Phi^i\Phi^k rdrd\phi\\&+\sum_k\theta^{t+1}_k\int_{\Omega_1}\bar{k}\left[\frac{\partial\Phi^i}{\partial r}\frac{\partial\Phi^k}{\partial r}+\frac{1}{r^2}\frac{\partial\Phi^i}{\partial r}\frac{\partial\Phi^k}{\partial r}\right]rdrd\phi\\&+\int_{\Gamma_1}\Phi^i Bi\theta^{t+1}d\Gamma-\frac{\omega\epsilon_0E_0^2R^2}{2k_0T_0}\\&\int_{\Omega_1}\kappa''(\theta^{t+1})\left\{\left(\sum_k E^{R,\,t+1}_{z,k}\Phi^k\right)^2+\left(\sum_k E^{I,\,t+1}_{z,k}\Phi^k\right)^2\right\}\Phi^i rdrd\phi\end{aligned} \tag{68}$$

For the field equations the weak forms for each of the domains Ω_1 and Ω_2 are added, thereby satisfying the boundary conditions given by Eq. 26 on Γ_1. For cylindrical samples the RBC is applied to the cylinder itself. The derivatives of the electric field in the surface integrals of Eqs. 66 and 67 are replaced by the expressions in Eqs. 48 and 49. In Eq. 68 an implicit backward difference is used to discretize the time domain resulting in an unconditionally stable algorithm. The thermal properties are assumed to be temperature-independent. The Newton-Raphson iterative procedure is used to solve for the electric field components and the temperature. At each time step the linear ($3N\times 3N$) system solved is:

$$\boldsymbol{J}(u^{n,t+1})\delta^{n,t+1}=-\boldsymbol{R}(u^{n,t+1}) \tag{69}$$

where

n = Newton iterate index
t = time index

where the Jacobian $\boldsymbol{J}$ consists of derivatives of the residuals with respect to the unknown coefficients, $J_{i,j}=\partial R_i/\partial u_j$, $\boldsymbol{u}$ is the vector of unknown coefficients, and $\delta^{n,t+1}$ is the update vector. The method is started with an initial guess and at each Newton iterate the solution is updated by $u^{n+1,t+1}=\delta^{n,t+1}+u^{n,t+1}$ till convergence is reached.

Residual equations: TE^z polarization

The analysis for the case of the transverse electric wave follows in a similar manner. Here the Galerkin finite element method yields the following residual equations. Expanding the real (H^R_l) and imaginary components (H^I_l) of the magnetic field, and the temperature (θ) in the basis Φ,

$$\tilde{H}^R_{z,l}=\sum_{k=1}^{N}H^R_{z,k}\Phi^k(r),\quad \tilde{H}^I_{z,l}=\sum_{k=1}^{N}H^I_{z,k}\Phi^k(r)$$

and

$$\tilde{\theta}=\sum_{k=1}^{N}\theta_k(\tau)\Phi^k(r) \tag{70}$$

the Galerkin finite element method yields the following residual equations for Eqs. 32, 33 and 52, respectively.

$$\begin{aligned}R_i^{(1)}=&\sum_k H^{R,\,t+1}_{z,k}\int_{\Omega}\psi^H_l\left[\frac{\partial\Phi^i}{\partial r}\frac{\partial\Phi^k}{\partial r}+\frac{1}{r^2}\frac{\partial\Phi^i}{\partial r}\frac{\partial\Phi^k}{\partial r}\right]rdrd\phi\\&-k_0^{*2}\sum_k H^{R,\,t+1}_{z,k}\int_{\Omega}\Phi^i\Phi^k rdrd\phi\\&+\sum_k H^{I,\,t+1}_{z,k}\int_{\Omega}\chi^H_l\left[\frac{\partial\Phi^i}{\partial r}\frac{\partial\Phi^k}{\partial r}+\frac{1}{r^2}\frac{\partial\Phi^i}{\partial r}\frac{\partial\Phi^k}{\partial r}\right]rdrd\phi\\&-\int_{\Gamma_2}\Phi^i\frac{\partial H^{R,\,t+1}_{z,2}}{\partial r}d\Gamma\end{aligned} \tag{71}$$

$$\begin{aligned}R_i^{(2)}=&\sum_k H^{I,\,t+1}_{z,k}\int_{\Omega}\psi^H_l\left[\frac{\partial\Phi^i}{\partial r}\frac{\partial\Phi^k}{\partial r}+\frac{1}{r^2}\frac{\partial\Phi^i}{\partial r}\frac{\partial\Phi^k}{\partial r}\right]rdrd\phi\\&-k_0^{*2}\sum_k H^{I,\,t+1}_{z,k}\int_{\Omega}\Phi^i\Phi^k rdrd\phi\end{aligned}$$

$$- \sum_k H_{z,k}^{R,t+1} \int_\Omega \chi_l^H \left[\frac{\partial \Phi^i}{\partial r} \frac{\partial \Phi^k}{\partial r} + \frac{1}{r^2} \frac{\partial \Phi^i}{\partial r} \frac{\partial \Phi^k}{\partial r} \right] r dr d\phi$$

$$- \int_{\Gamma_2} \Phi^i \frac{\partial H_{z,2}^{I,t+1}}{\partial r} d\Gamma \tag{72}$$

$$R_i^{(3)} = \sum_k \int_{\Omega_1} \overline{\rho C_p} \left\{ \frac{\theta_k^{t+1} - \theta_k^t}{\Delta \tau} \right\} \Phi^i \Phi^k r dr d\phi$$

$$+ \sum_k \theta_k^{t+1} \int_{\Omega_1} \overline{k} \left[\frac{\partial \Phi^i}{\partial r} \frac{\partial \Phi^k}{\partial r} + \frac{1}{r^2} \frac{\partial \Phi^i}{\partial r} \frac{\partial \Phi^k}{\partial r} \right] r dr d\phi$$

$$+ \int_{\Gamma_1} \Phi^i Bi \theta^{t+1} d\Gamma - \frac{\omega \epsilon_0 E_0^2}{2 k_0 T_0 k_0^{*2}} \int_{\Omega_1} \chi_1^H \left[\left(\frac{\partial H_{z,1}^I}{\partial r} \right)^2 \right.$$

$$\left. + \left(\frac{\partial H_{z,1}^R}{\partial r} \right)^2 + \left(\frac{1}{r} \frac{\partial H_{z,1}^I}{\partial \phi} \right)^2 + \left(\frac{1}{r} \frac{\partial H_{z,1}^R}{\partial \phi} \right)^2 \right] \Phi^i r dr d\phi \tag{73}$$

The boundary integrals in Eqs. 71 and 72 are replaced by the same expressions developed for the TM^z case. As in the previous case the boundary conditions given by Eq. 34 are satisfied by adding the weak forms for the two regions 1 and 2.

The finite element analysis for the electric field components $E_{\phi,l}^*$ and $E_{r,l}^*$ is outlined below. If $E_{\phi,l}^* = E_{\phi,l}^R + iE_{\phi,l}^I$ and $E_{r,l}^* = E_{r,l}^R + iE_{r,l}^I$, then the dimensionless equations for the electric field components by equating the real and imaginary components from Eqs. 35 and 36 are:

$$E_{\phi,l}^R = \frac{1}{k_0^*} \left[\psi_l^H \frac{\partial H_{z,l}^I}{\partial r} - \chi_l^H \frac{\partial H_{z,l}^R}{\partial r} \right] \tag{74}$$

$$E_{\phi,l}^I = \frac{-1}{k_0^*} \left[\psi_l^H \frac{\partial H_{z,l}^R}{\partial r} + \chi_l^H \frac{\partial H_{z,l}^I}{\partial r} \right] \tag{75}$$

$$E_{r,l}^R = \frac{1}{r k_0^*} \left[- \psi_l^H \frac{\partial H_{z,l}^I}{\partial \phi} + \chi_l^H \frac{\partial H_{z,l}^R}{\partial \phi} \right] \tag{76}$$

$$E_{r,l}^I = \frac{1}{r k_0^*} \left[\psi_l^H \frac{\partial H_{z,l}^R}{\partial \phi} + \chi_l^H \frac{\partial H_{z,l}^I}{\partial \phi} \right] \tag{77}$$

Using the expansions given in Eq. 70 and

$$\tilde{E}_{\phi,l}^R = \sum_{j=1}^N E_{\phi,j}^R \Phi^j(r) \tag{78}$$

the Galerkin weak form for Eq. 74 is:

$$\sum_j E_{\phi,j}^R \int_\Omega \Phi^i \Phi^j d\Omega = \sum_j H_{z,j}^I \int_\Omega \frac{\psi_l^H}{k_0^*} \Phi^i \frac{\partial \Phi^j}{\partial r} d\Omega$$

$$- \sum_j H_{z,j}^R \int_\Omega \frac{\chi_l^H}{k_0^*} \Phi^i \frac{\partial \Phi^j}{\partial r} d\Omega. \tag{79}$$

Once the magnetic field is known, the righthand side of Eq. 79 can be evaluated and can be written as a set of linear algebraic equations:

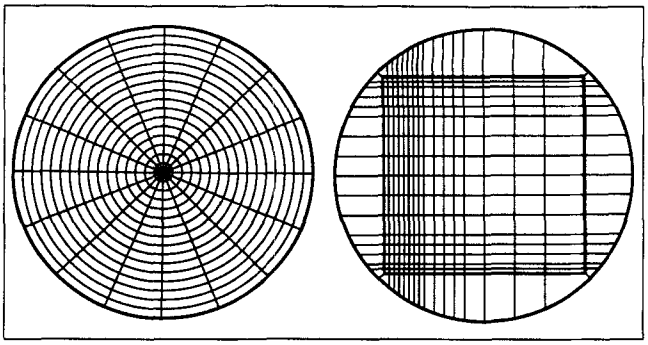

Figure 2. Example of meshes used in finite element analysis for the cylindrical and square samples.

$$Au = f, \tag{80}$$

where

$$A_{i,j} = \int_\Omega \Phi^i \Phi^j d\Omega$$

$$u_j = E_{\phi,j}^R$$

$$f_i = \sum_j H_{z,j}^I \int_\Omega \frac{\psi_l^H}{k_0^*} \Phi^i \frac{\partial \Phi^j}{\partial r} d\Omega - \sum_j H_{z,j}^R \int_\Omega \frac{\chi_l^H}{k_0^*} \Phi^i \frac{\partial \Phi^j}{\partial r} d\Omega. \tag{81}$$

The other electric field components can be evaluated in a similar manner. The complex forms of Eqs. 35 and 36 could also have been used to evaluate the electric field.

Discretization, integrations and convergence criterion

The heating of samples of circular and square cross-section exposed to transverse magnetic and transverse electric plane waves were studied. Finite element meshes used for both geometries are shown in Figure 2.

Mesh numbering from the center outward was used in both cases. For the cylindrical sample the convection boundary condition for the heat equation, Eq. 52 and the RBCs are imposed on Γ_1. In the case of the square sample the RBC is imposed on Γ_2.

The domain integrals in the residual equations are evaluated using nine node biquadratic basis functions by mapping the global element $\rho - \phi$ domain isoparametrically onto the unit square $\xi - \eta$ domain (Strang and Fix, 1973) using:

$$\rho = \sum_{i=1}^9 \rho_i \Phi_i(\xi, \eta) \quad \text{and} \quad \phi = \sum_{i=1}^9 \phi_i \Phi_i(\xi, \eta) \tag{82}$$

where $0 \le \xi \le 1$, $0 \le \eta \le 1$ and $\Phi_i(\xi, \eta)$ are the local biquadratic basis functions on the $\xi - \eta$ domain. For the case of the cylindrical sample collapsed elements are used where three nodes share the co-ordinates at the origin.

The mesh design was such that elements could be added and removed depending on the nature of the solution. Figure 2b illustrates the mesh used for a large sample where the power

deposition is primarily at the incident face and at the sample corners. Typically 144 elements were used, and 95% of the time was spent solving the linear set of equations at each Newton iterate. For the cylindrical sample a banded solver was used, and for the square rod the LINPACK full solver was found to be faster than the YALE sparse matrix solver. However, when the number of elements exceeded about 256, YALE performed better than LINPACK. Convergence for each Newton step was based on the $\mathcal{L}_2$ norm of the residuals with a convergence criterion of 10^{-9}. To start the Newton scheme a very small time step, $\Delta t = 1 \times 10^{-4}$ s was used. After the first time step, the time step was increased to 5 – 10 s.

Evaluation of global RBC

As an example of how the RBC is incorporated in the analysis, consider the surface integral in Eq. 66. Using the expressions for the radiation boundary condition, Eq. 48, with the finite element expansions for the real and imaginary electric field components and exchanging integration and summation signs the surface integral in Eq. 66 reduces to:

$$\int_{\Gamma_2} \Phi^i \frac{\partial E^R_{z,2}}{\partial r}\, d\Gamma = \sum_n Re(C_n)\xi_{in} + \sum_j E^R_{z,j} \sum_n Re(D_n)[\xi^c_{in}\xi^c_{jn} + \xi^s_{in}\xi^s_{jn}] - \sum_j E^I_{z,j} \sum_n Im(D_n)[\xi^c_{in}\xi^c_{jn} + \xi^s_{in}\xi^s_{jn}] \quad (83)$$

where

$$\left.\begin{aligned} \xi^c_{ln} &= \int_0^{2\pi} \cos n\theta \Phi^l d\theta \\ \xi^s_{ln} &= \int_0^{2\pi} \sin n\theta \Phi^l d\theta \end{aligned}\right\} \quad l = i,j \quad (84)$$

The integrals in Eq. 84 are evaluated analytically and the summations over the index, n, are performed once for each computation. The other surface integrals are evaluated in a similar manner.

Results and Discussion

The accuracy of the numerical solution of Maxwell's equations was tested with the analytical solution for the power in the cylindrical sample. Figure 3 illustrates the comparison for a 144-element mesh having equal spacing in the r and θ direction. The finite element solution is within 1% of the analytical solution. For cases where the sample dimensions were large compared to the wavelength of radiation in the medium, 256 elements were needed to achieve the same degree of accuracy. Figure 3 also illustrates the comparison of powers for the TE^z case. Here the contours, though qualitatively accurate, are not as well resolved as in the previous case. The electric field values are obtained by the solution method outlined earlier. Though the magnetic field intensities were accurate to less than 1% when compared with the analytical solutions, the electric field values were within a few percent of the exact solution. This is due to the fact the the derivatives of the electric field are

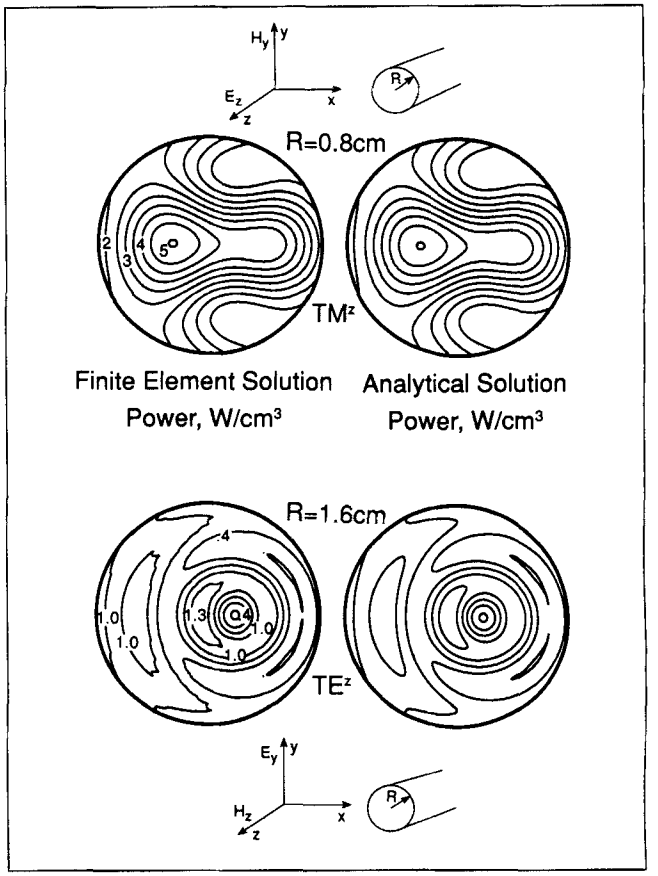

Figure 3. Comparison of microwave power from the finite element solution to Maxwell's equations and the analytical solution for TM^z and TE^z polarization.

$f = 2{,}800$ MHz, $I_0 = 3$ W·cm^{-2}, $\kappa'' = 13.1$, $\kappa' = 42.6$.

discontinuous across element boundaries for the biquadratic basis functions used. A similar situation arises when evaluating heat fluxes from temperature fields. Apart from serving as a test, this loss in accuracy does not effect the temperature contours as the derivatives of the magnetic field components are evaluated only at the Gauss points within each element while computing the integrals involving the power term in the TE^z case. As a second check, the electric field values for both the TM^z and TE^z polarizations were compared with the finite difference time domain solutions of Maxwell's equations by Borup et al. (1987). The comparison was very good for both the polarizations.

The intensity of the incident plane wave, I_0, used in the simulation is 3 W·cm^{-2} and is related to the incident electric field intensity E_0 by:

$$I_0 = \frac{1}{2} c\epsilon_0 E_0^2 \quad (85)$$

A heat-transfer coefficient, $h = 10$ W·m^{-2}·K^{-1}, was used for the calculations in Figures 5 and 8, and $h = 0$ was used for the other heat-transfer simulations. The Biot numbers corresponding to these values of h varied between 0 and 1. For this range of Biot numbers the effect of surface cooling was small. The

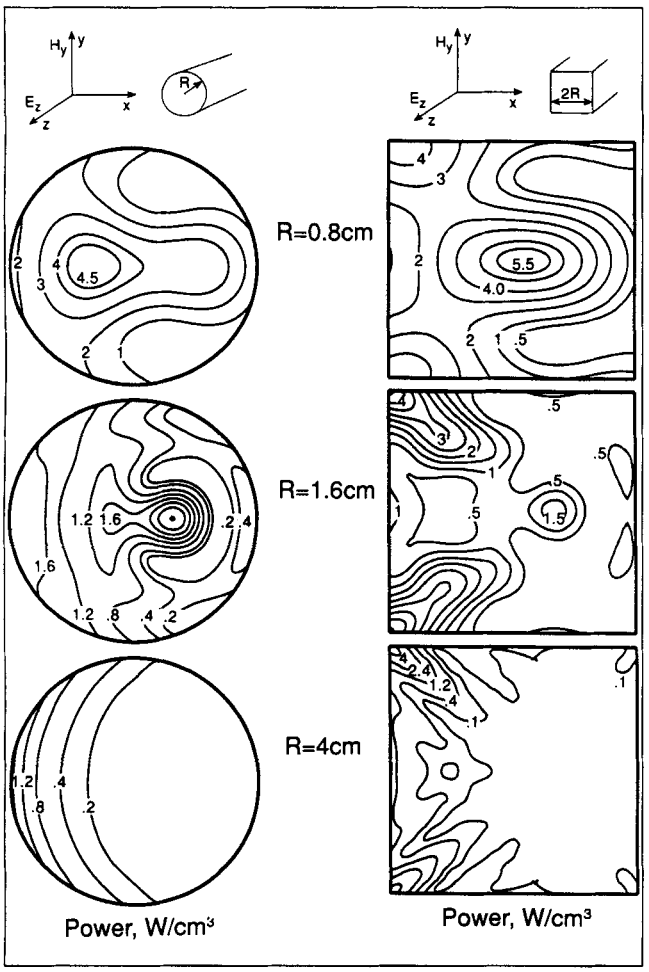

Figure 4. Comparison of power contours for cylindrical and square rods exposed to *TM*^{z} polarized plane waves.

$f = 2{,}800$ MHz, $I_0 = 3\ \mathrm{W \cdot cm^{-2}}$, $\kappa'' = 13.1$, $\kappa' = 42.6$.

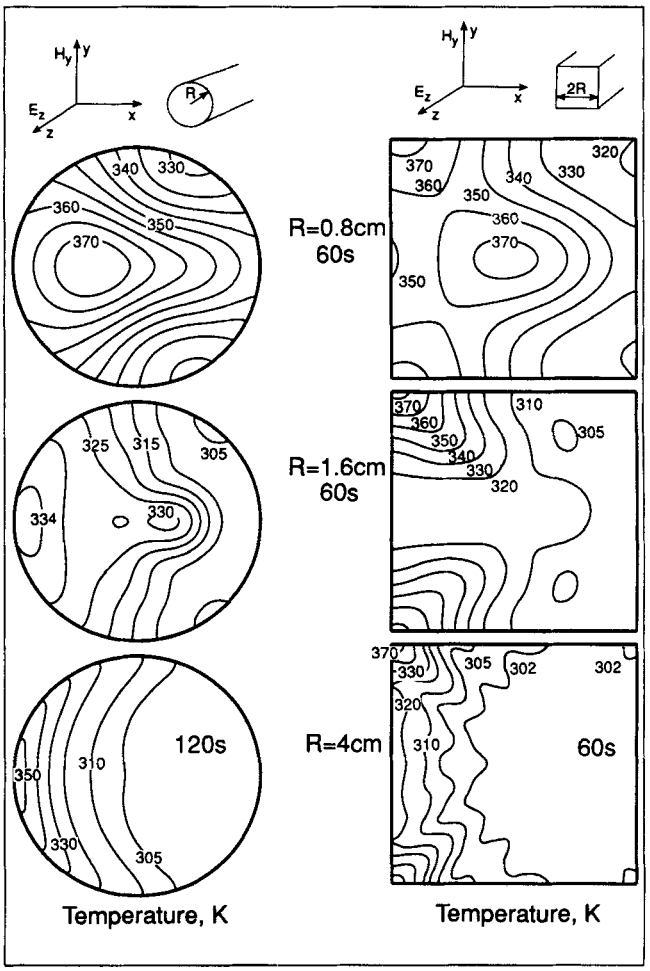

Figure 5. Comparison of temperature contours for cylindrical and square rods whose power distributions are shown in Figure 4.

$k = 0.491\ \mathrm{W \cdot m^{-1} \cdot K^{-1}}$, $\rho = 1{,}070\ \mathrm{kg \cdot m^{-3}}$, $C_p = 2{,}510\ \mathrm{J \cdot kg^{-1} \cdot K^{-1}}$.

ambient temperature was 300 K, and the sample was held at this temperature prior to exposure to microwaves.

One of the factors of concern in microwave processing is the focusing of energy by corners and edges (Datta, 1990). Figure 4 compares power distributions for rods of square and cylindrical cross-sections. Material dielectric properties are those of raw beef (Ohlsson and Bengtsson, 1975). The frequency of the incident plane waves is 2,800 MHz, and at this frequency the variation of dielectric properties with temperature is small and has a negligible influence on heating (Ayappa et al., 1991). The wavelength of radiation (λ_m) in the sample is 1.621 cm, and the penetration depth is 1.717 cm. The location of maximum power peak in the cylindrical samples depends on the radius of the sample.

For the $R = 0.8$ cm sample the peak is seen closer to the incident face, and for the $R = 1.6$ cm sample the peak is shifted away from the incident face. In general for smaller samples the maximum value of power absorbed is higher, and for samples much smaller than the wavelength (not shown in the figure) the power distribution is uniform. For larger samples as in the case of the $R = 4$ cm cylinder the power decays from the incident face into the sample and no strong interference effects are observed. Here the sample diameter is about 4.75 time the penetration depth.

Kritikos and Schwan (1975) have studied the distribution of power in spheres exposed to plane waves. Maximum power was found to be absorbed inside the sphere or at the surface of the sphere depending on the magnitude of the wavelength and radius of the sphere. Unlike in the case of the cylinder, strong resonant conditions, during which power absorption was a maximum, was found for the spheres.

The power distributions for the square samples whose sides are of length $2R$ make an interesting comparison with the cylindrical samples of the same diameter. The effect of the corners is more pronounced for the $R = 1.6$ and $R = 4$ cm samples. For the larger samples microwaves penetrate about 1 to 2 cm from the corners and is independent of the sample size. A similar trend was observed in the experiments performed by Risman et al. (1987) in a domestic oven. For the $R = 0.8$ cm sample, though power is being deposited at the corners, a significant amount is being absorbed at the sample center as well. For very small samples as in the case of the cylinder, the power distribution is uniform and both approach the same limit as the radius is decreased. Thus for samples whose di-

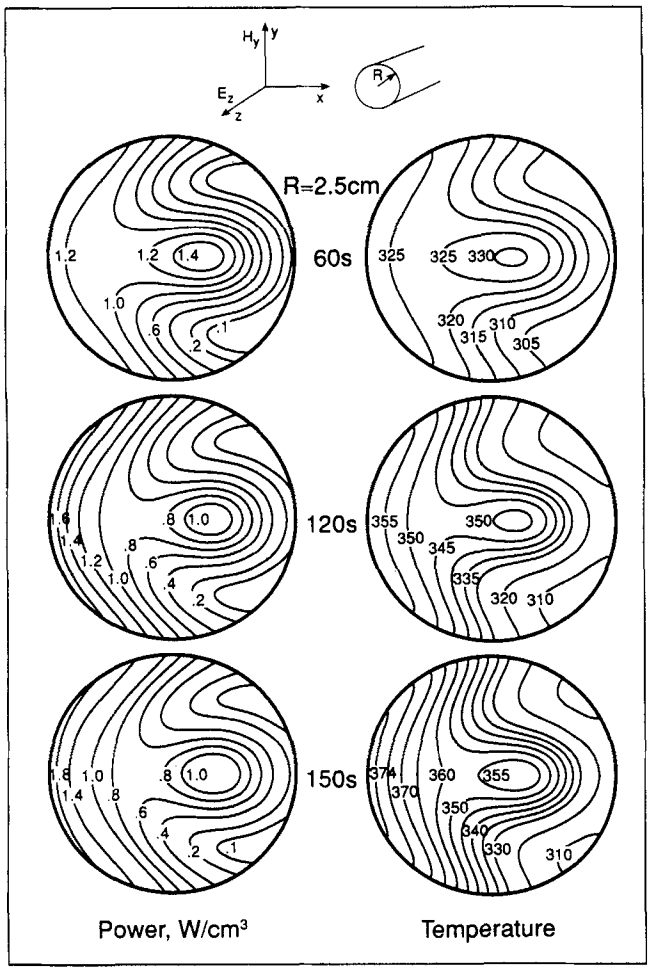

Figure 6. Power and temperature distributions for a beef sample with temperature-dependent dielectric properties.

See table for dielectric data (Ohlsson and Bengtsson, 1975).
$f = 900$ MHz, $I_0 = 3$ W·cm^{-2}, $k = 0.491$ W·m^{-1}·K^{-1}, $\rho = 1{,}070$ kg·m^{-3}, $C_p = 2{,}510$ J·kg^{-1}·K^{-1}.

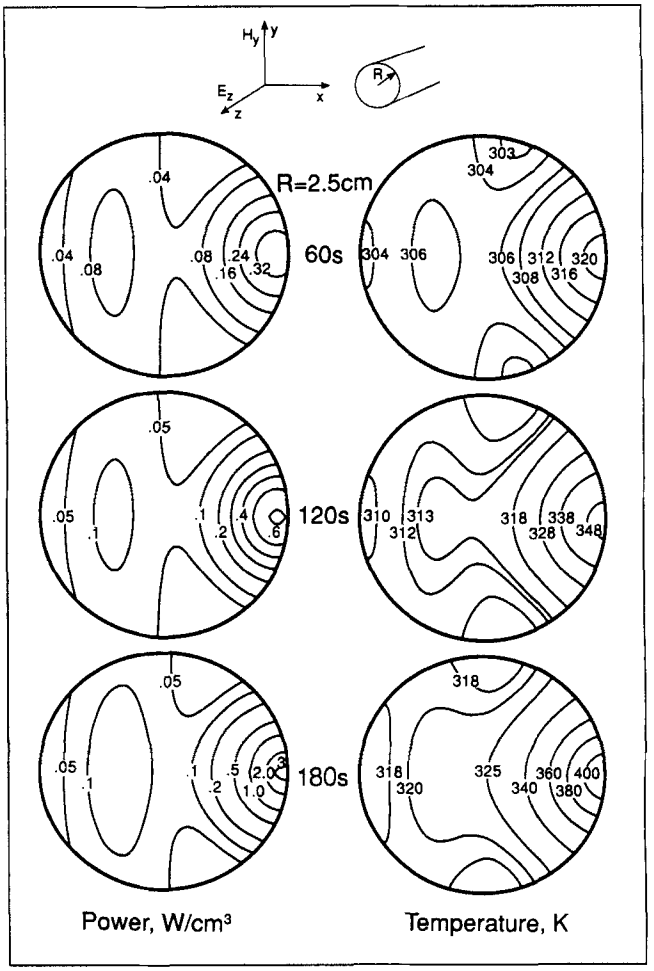

Figure 7. Power and temperature distributions for Nylon 66 illustrating a runaway effect.

See table for dielectric data (Huang, 1976).
$f = 3{,}000$ MHz, $I_0 = 3$ W·cm^{-2}, $k = 0.43$ W·m^{-1}·K^{-1}, $\rho = 1{,}200$ kg·m^{-3}, $C_p = 520$ J·kg^{-1}·K^{-1}.

mensions are much smaller than the wavelength, corners have a negligible effect.

For larger samples the microwave power deposited differs significantly for the two shapes. Figure 5 illustrates the temperature contours for the power distribution shown in Figure 4. Qualitative aspect of the temperature contours follow from the power distributions. The edges for the $R = 0.8$ cm sample have a small effect on the temperature distribution and heating occurs in the sample interior as well. For the $R = 1.6$ cm sample most of heating occurs at the corners. The amount of power deposited at the corners and consequently the temperatures in the vicinity of the corners are independent of the dimensions of the samples shown in Figure 5. For the $R = 4$ cm sample, heating in the interior of the sample must take place mostly by conduction from the incident face, as the power is absorbed within the first few cms. In these situations, power cycling or sample rotation would help to smooth out hot spots and produce a more even temperature distribution.

The influence of temperature dependence of dielectric properties is illustrated in Figures 6 and 7. The temperature-dependent properties used for Figure 6 are those for raw beef at 900 Mhz (Ohlsson and Bengtsson, 1975). The data were fit to a polynomial using the method of least squares (Tables 1 and 2). The primary effect due to the temperature dependence is the decreasing penetration depth as the sample heats. Power and temperature profiles are illustrated in Figure 6 at 60, 120 and 150 s. At the onset of heating due to the higher penetration depth most of the power is deposited away from the incident face of the sample giving rise to a hot spot. Even though the dielectric loss increases with temperature, after 120 s the power deposited at the hot spot decreases and more power is absorbed at the incident face of the sample. The effect is stronger at 150 s where the temperature rise at the hot spot is only 5 degrees in contrast to a 20 degree rise from 60 to 120 s. At 150 s due to the decreasing penetration depth, the incident face heats up much faster than the interior. Such nonlinear effects tend to smooth out the temperature in the sample as seen at 120 s.

Figure 7 illustrates a runaway effect for Nylon 66 whose dielectric loss is a strong function of temperature, increasing rapidly around 400 K (Huang, 1976). In such situations a hot

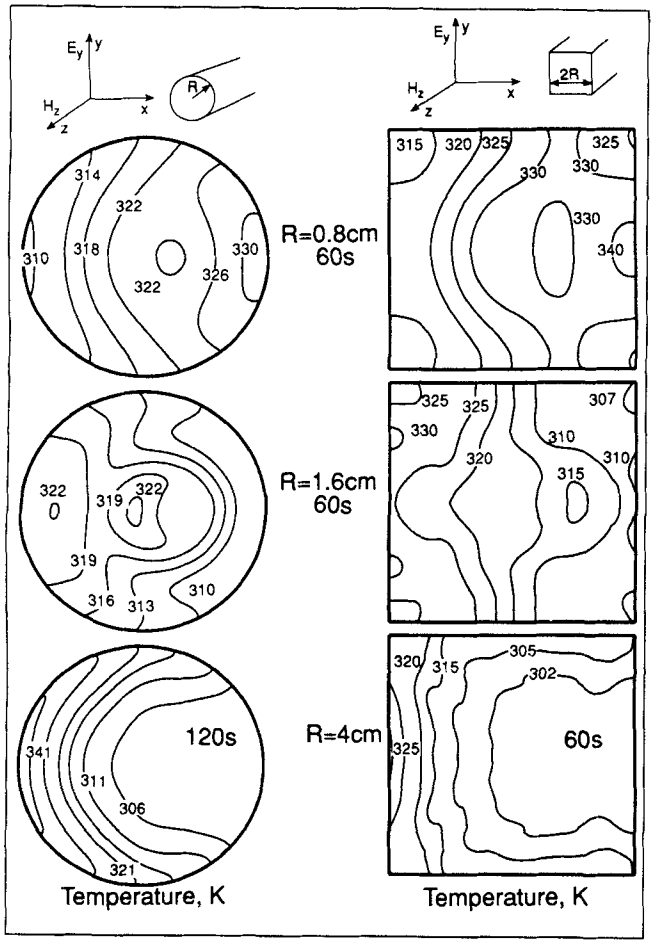

Figure 8. Comparison of temperature contours for cylindrical and square rods exposed to TE^z polarized plane waves.

f=2,800 MHz, I_0=3 W·cm^{-2}, κ''=13.1, κ'=42.6, k=0.491 W·m^{-1}·K^{-1}, ρ=1,070 kg·m^{-3}, C_p=2,510 J·kg^{-1}·K^{-1}.

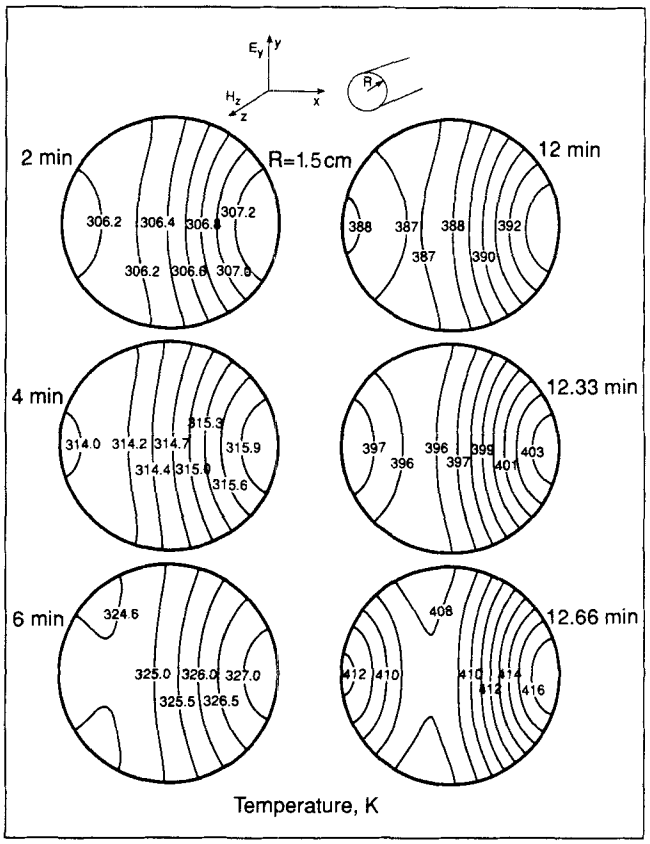

Figure 9. Power and temperature distributions for Nylon 66 illustrating the runaway heating effects for the case of TE^z polarization.

See table for dielectric data (Huang, 1976).
f=3,000 MHz, I_0=3 W·cm^{-2}.

spot can easily become a runaway hot spot during microwave heating. Figure 7 shows the power and corresponding temperature profiles for a sample of radius 2.5 cm. A power peak is present at the end away from the incident face. During the first 2 min the power increases to about 0.6 W·cm^{-3} creating a hot spot. During the 3rd minute of heating the power absorbed increases significantly and the temperature rises sharply.

So far, all the results discussed have been for the TM^z polarization where the electric field is polarized along the long axis of the sample. Results for the TE^z polarization, where the magnetic field is polarized along the long axis of the sample, are discussed next. Here all the parameters are similar to those used for Figures 5 and 7. Figure 8 shows the temperature patterns for the same sample used in the simulation of Figure 5. Though the power contours are not shown for this case the temperature contours are in agreement with the nature of the power contours obtained analytically for the cylinder. Apart from the difference in the distribution of power, the temperatures are much lower here for the same amount of heating. Thus the coupling with the field is less than in the case of TM^z polarization. This difference in power absorption for the two polarizations has been studied by Massoudi et al. (1979) for

Table 1. Dielectric Constant, κ': $\kappa' = a_0 + a_1 T + a_2 T^2 + a_3 T^3$. ($T$, K)

Material	f (MHz)	a_0	a_1	a_2	a_3
Raw Beef	900	82.23	−0.1059		
Nylon	3,000	16.727	−0.10279	2.4192×10^{-4}	-1.7592×10^{-7}

Table 2. Dielectric Loss, κ'', data (Ohlsson and Bengtsson, 1975): $\kappa'' = b_0 + b_1 T + b_2 T^2 + b_3 T^3 + b_4 T^4$. ($T$, K)

Material	f (MHz)	b_0	b_1	b_2	b_3	b_4
Raw Beef	900	236.85	−1.527	2.7277×10^{-3}		
Nylon	3,000	84.16	−1.0011	4.4563×10^{-3}	-8.8029×10^{-6}	6.5208×10^{-9}

cylindrical samples based on analytical solutions for the field. For cylindrical samples the induced field for the TE^z polarization is a function of the properties of the medium. The phi component of the electric field is continuous at the boundaries of the sample, but the radial component is reduced by the value proportional to the complex permittivity of the medium. In the case of the TM^z wave, the electric field is continuous across the interface and therefore couples more effectively with the sample. Further, their results indicate that at lower frequencies for the same sample dimensions, the power absorption for the TM^z polarization increases monotonically as the frequency is decreased. This is somewhat similar to the situation in which the sample radius is decreased for a fixed frequency. The same trend was observed while reducing the sample thickness in this study. Johnson et al. (1979) have observed that for the TM^z case their power absorbed is higher increasing for longer thinner objects and decreasing for shorter fatter objects. Also the corners focus heat but not to the same extent as in the case of the TM^z wave. Figure 9 illustrates the runaway heating effect for the Nylon 66 sample. After the 12th min the sample temperature rises sharply by about 10 degrees for every 20 s. Contrast the heating rates with the TM^z case.

Conclusion

Using Galerkin finite elements we have predicted temperature distributions of long lossy rods exposed to an incident plane wave. The method uses a radiation boundary condition imposed on a cylindrical boundary to contain the domain of the analysis. This technique minimizes the need to discretize the space surrounding the sample. Maxwell's equations and the heat equations are solved simultaneously on the same grid using the finite element method. The technique allows the analysis of materials with temperature-dependent properties in a straightforward manner, and the resulting nonlinear equations are solved using Newton's iteration. The method facilitates the incorporation of the RBC, and temperature distributions for both polarizations can be predicted.

In the cylindrical samples the distribution of power is a strong function of the cylinder radius. For smaller samples, the magnitude and location of the power peak vary with the radius of the cylinder. Focusing was found to be stronger for the TM^z polarization than the TE^z polarization. In both cases, however, for thick cylinders, heating occurred primarily at the incident face.

Comparison of samples of cylindrical and square cross-section indicates that the corners heat up rapidly, significantly altering the temperature distributions. This is pronounced if the sample dimension is large compared to the wavelength of radiation in the medium. In cases where uniformity of product temperature is of importance, this study indicates that corners and edges should be avoided or rounded off to minimize localized heating.

Temperature dependence of the dielectric properties alters the distribution of power as the sample heats. Heating is illustrated with materials whose decreasing penetration depth is the dominant effect and where the increasing dielectric loss leads to a runaway effect.

In addition to sample dimensions and geometry, the polarization of the incident waves influences the temperature distribution. For the TM^z polarization, the sample couples strongly with the field giving a higher deposited power when compared with the TE^z polarization. Further, the power deposited for the TM^z polarization is higher as the sample gets thinner and decreases for thicker samples.

Acknowledgment

We thank Kraft General Food Inc. for financial support and the Minnesota Supercomputer Institute for computing resources.

Notation

B = magnetic induction, $Wb \cdot m^{-2}$
Bi = Biot number
c = velocity of light, $m \cdot s^{-1}$
C_p = specific heat capacity, $J \cdot kg^{-1} \cdot K^{-1}$
D = electric displacement, $C \cdot m^{-2}$
E = electric field intensity, $V \cdot m^{-1}$
f = frequency of incident radiation, Hz
h = heat-transfer coefficient, $W \cdot m^{-2} \cdot K^{-1}$
H = magnetic field intensity, $Amp \cdot m^{-1}$
J = current flux, $Amp \cdot m^{-2}$
k = thermal conductivity, $W \cdot m^{-1} \cdot K^{-1}$
k_0 = reference thermal conductivity, $W \cdot m^{-1} \cdot K^{-1}$
k_0 = free space propagation constant, m^{-1}
p = microwave source term, $W \cdot m^{-3}$
P = dimensionless microwave source term
r = dimensionless radial distance
R = radius of sample, m
t = time, s
T = temperature, K
T_0 = initial temperature, K
T_∞ = ambient temperature, K
E^I = dimensionless imaginary electric field component
E^R = dimensionless real electric field component
H^I = dimensionless imaginary magnetic field component
H^R = dimensionless real magnetic field component

Greek letters

α = phase constant, m^{-1}
α_0 = reference thermal diffusivity, $m^2 \cdot s^{-1}$
σ_0 = free space phase constant, m^{-1}
β = attenuation constant, m^{-1}
γ = dimensionless propagation constant
ϵ = permittivity, $Farad \cdot m^{-1}$
ϵ_0 = free space permittivity, $Farad \cdot m^{-1}$
ϵ' = dielectric constant, $Farad \cdot m^{-1}$
ϵ'' = dielectric loss factor, $Farad \cdot m^{-1}$
ϵ^* = complex permittivity, $Farad \cdot m^{-1}$
θ = dimensionless temperature
κ = relative permittivity
κ' = relative dielectric constant
κ'' = relative dielectric loss
κ^* = complex relative permittivity
λ = wavelength, m
λ_m = wavelength in the medium, m
μ = permeability, $He \cdot m^{-1}$
μ_0 = free space permeability, $He \cdot m^{-1}$
ρ = density, $kg \cdot m^{-3}$
ρ = radial distance
ρ_0 = reference density, $kg \cdot m^{-3}$
σ = electric conductivity, $mho \cdot m^{-1}$
τ = dimensionless time
ϕ = basis functions
ω = angular frequency, $Rad \cdot s^{-1}$

Subscripts

l = layer

Superscripts

n = Newton iterate index
I = imaginary field quantity
R = real field quantity
t = time index
$*$ = dimensionless quantity

Literature Cited

Abramowitz, M., and I. A. Stegun, *Handbook of Mathematical Functions*, 9th ed., Dover, New York (1970).

Ayappa, K. G., H. T. Davis, E. A. Davis, and J. Gordon, "Analysis of Microwave Heating of Materials with Temperature Dependent Properties," *AIChE J.*, **37**, 313 (1991).

Balanis, C. A., *Advanced Engineering Electromagnetics*, Wiley, New York (1989).

Bayliss, A., and E. Turkel, "Radiation Boundary Conditions for Wave Like Equations," *Commun. Pure Appl. Math.*, **33**, 707 (1980).

Blaschak, J. G., and G. A. Kriegsmann, "A Comparative Study of Absorbing Boundary Conditions," *J. of Comp. Phys.*, **77**, 109 (1988).

Borup, D. T., D. M. Sullivan, and O. P. Gandhi, "Comparison of the FFT Conjugate Gradient Method and the Finite-Difference Time-Domain Method for the 2-D Absorption Problem," *IEEE Trans. Microwave Theory Tech.*, **35**, 383 (1987).

Brandrup, J., and E. H. Immergut, *Polymer Handbook*, 3rd ed., Wiley, New York (1989).

Britt, C. L., "Solution of Electromagnetic Scattering Problems Using Time Domain Techniques," *IEEE Trans. Antennas and Propagat.*, **37**, 1181 (1989).

Bussey, H. E., and J. H. Richmond, "Scattering by a Lossy Dielectric Circular Cylindrical Multilayer, Numerical Values," *IEEE Trans. Antennas Propagat.*, **23**, 723 (1975).

Cangellaris, A. C., C. Lin, and K. K. Mei, "Point-Matched Time Domain Finite Element Methods for Electromagnetic Radiation and Scattering," *IEEE Trans. Antennas and Propagat.*, **35**, 1160 (1987).

Chabinsky, I. J., "Applications of Microwave Energy Past, Present and Future Brave New Worlds," *Mat. Res. Symp. Proc.*, **124**, 17 (1988).

Chang, S., and K. K. Mei, "Application of the Unimoment Method to Electromagnetic Scattering of Dielectric Cylinders," *IEEE Trans. Antennas and Propagat.*, **24**, 35 (1976).

D'Angelo, J., and I. D. Mayergoyz, "On the Use of Local Absorbing Boundary Conditions for RF Scattering Problems," *IEEE Trans. Magnetics*, **25**, 3040 (1989).

Datta, A. K., "Heat and Mass Transfer in the Microwave Processing of Food," *Chem. Eng. Prog.*, **6**, 47 (1990).

De Wagter, C., "Computer Simulation Predicting Temperature Distributions Generated by Microwave Absorption in Multilayered Media," *J. Microwave Power*, **19**, 97 (1984).

Gandhi, O. P., "Frequency and Orientation Effects on Whole Animal Absorption of Electromagnetic Waves," *IEEE Trans. Biomed. Eng.*, **22**, 536 (1975).

Glisson, A. W., "Recent Advances in Frequency Domain Techniques for Electromagnetic Scattering Problems," *IEEE Trans. Magnetics*, **25**, 2867 (1989).

Huang, H., "Temperature Control in a Microwave Resonant Cavity System for Rapid Heating of Nylon Monofilament," *J. Microwave Power*, **11**, 305 (1976).

Johnson, C. C., C. H. Durney, P. W. Barber, H. Massoudi, S. J. Allen, and J. C. Mitchell, "Descriptive Summary: Radio-Frequency Radiation Dosimetry Handbook," *Radio Sci.*, **14**, 57 (1979).

Jolly, P., and I. Turner, "Non-Linear Field Solutions of One-Dimensional Microwave Heating," *J. Microwave Power and EM Energy*, **25**, 3 (1990).

Jow, J., M. C. Hawley, M. Finzel, and T. Kern, "Dielectric Analysis of Epoxy/Amine Resins Using Microwave Cavity Technique," *Polym. Eng. and Sci.*, **28**, 1450 (1988).

Keller, J. B., and D. Givoli, "Exact Non-Reflecting Boundary Conditions," *J. Comp. Phys.*, **82**, 172 (1989).

Kritikos, H. N., and H. P. Schwan, "The Distribution of Heating Potential Inside Lossy Spheres," *IEEE Trans. Biomed. Eng.*, **22**, 457 (1975).

Le Van, Q., and A. Gourdenne, "Microwave Curing of Epoxy Resins with Diaminodiphenylmethane: I. General Features," *Eur. Polym. J.*, **23**, 777 (1987).

Lee, R. L., and N. K. Madsen, "A Mixed Finite Element Formulation for Maxwell's Equations in the Time Domain," *J. Comput. Phys.*, **88**, 284 (1990).

Livesay, D. E., and K. Chen, "Electromagnetic Fields Induced Inside Arbitrarily Shaped Biological Bodies," *IEEE Trans. Microwave Theory Techn.*, **22**, 1273 (1974).

Lynch, D. R., K. D. Paulsen, and J. W. Strohbehn, "Finite Element Solution of Maxwell's Equations for Hyperthermia Treatment Planning," *J. of Comput. Phys.*, **58**, 246 (1985).

Lynch, D. R., K. D. Paulsen, and J. W. Strohbehn, "Hybrid Finite Element for Unbounded Electromagnetic Problems in Hyperthermia," *Int. J. Numer. Methods Eng.*, **23**, 1915 (1986).

Marin, S. P., "Computing Scattering Amplitudes for Arbitrary Cylinders Under Incident Plane Waves," *IEEE Trans. Antennas Propagat.*, **30**, 1045 (1982).

Massoudi, H., C. H. Durney, P. W. Barber, and M. F. Iskander, "Electromagnetic Absorption in Multilayered Cylindrical Models of Man," *IEEE Trans. Microwave Theory Tech. MTT*, **27**, 825 (1979).

Massoudi, H., C. H. Durney, and C. C. Johnson, "A Geometrical-Optics and an Exact Solution for Internal Fields in and Energy Absorption by a Cylindrical Model of Man Irradiated by and Electromagnetic Plane Wave," *Radio Sci.*, **14**, 35 (1979).

Mittra, R., O. Ramahi, A. Khebir, R. Gordon, and A. Kouki, "A Review of Absorbing Boundary Conditions for Two and Three Dimensional Electromagnetic Scattering Problems," *IEEE Trans. on Magnetics*, **25**, 3034 (1989).

Nachman, M., and G. Turgeon, "Heating Patterns in Multi-layered Material Exposed to Microwaves," *IEEE Trans. Microwave Theory Tech.*, **32**, 547 (1984).

Ohlsson, T., and N. E. Bengtsson, "Dielectric Food Data for Microwave Sterilization," *J. Microwave Power*, **10**, 93 (1975).

Paulsen, K. D., D. R. Lynch, and J. W. Strobehn, "Three-Dimensional Finite, Boundary and Hybrid Element Solutions of the Maxwell Equations for Lossy Dielectric Media," *IEEE Trans. Microwave Theory Tech. MTT*, **36**, 682 (1988).

Pearson, L. W., "An Exact Radiation Boundary Condition for the Finite-Element Solution of Electromagnetic Scattering of an Open Domain," *IEEE Trans. on Magnetics*, **25**, 3046 (1989).

Peterson, A. F., and S. P. Castillo, "A Frequency-Domain Differential Equation Formulation for Electromagnetic Scattering from Inhomogeneous Cylinders," **37**, 601 (1989).

Richmond, J. H., "Scattering by a Dielectric Cylinder of Arbitrary Cross Section Shape," *IEEE Trans. Antennas Propagat.*, **12**, 334 (1963).

Risman, P. O., T. Ohlsson, and B. Wass, "Principles and Models of Power Density Distribution in Microwave Oven Loads," *J. Microwave Power*, **22**, 193 (1987).

Ruppin, R., "Electromagnetic Power Deposition in a Dielectric Cylinder in the Presence of a Reflecting Surface," *IEEE Trans. Microwave Theory Tech.*, **27**, 910 (1979).

Smyth, N. F., "Microwave Heating of Bodies with Temperature Dependent Properties," *Wave Motion*, **12**, 171 (1990).

Spiegel, R. J., "A Review of Numerical Models for Predicting the Energy Deposition and Resultant Thermal Response of Humans Exposed to Electromagnetic Fields," *IEEE Trans. Microwave Theory Tech.*, **32**, 730 (1984).

Sullivan, D. M., D. T. Borup, and O. P., Gandhi, "Use of Finite-Difference Time-Domain Method in Calculating EM Absorption in Human Tissues," *IEEE Trans. Biomedical Eng.*, **34**, 148 (1987).

Sullivan, D. M., O. P., Gandhi, and A. Taflove, "Use of Finite-Difference Time-Domain Method for Calculating EM Absorption in Man Models," *IEEE Trans. Biomedical Eng.*, **35**, 179 (1988).

Taflove, A., "Application of the Finite-Difference Time-Domain Method to Sinusoidal Steady-State Electromagnetic-Penetration Problems," *IEEE Trans. Electromagn. Compat.*, **22**, 191 (1980).

Taflove, A., and M. E. Brodwin, "Computation of the Electromagnetic Fields and Induced Temperatures within a Model of the Microwave Irradiated Human Eye," *IEEE Trans. Microwave Theory Tech.*, **23**, 888 (1975).

Taflove, A., and M. E. Brodwin, "Numerical Solution of Steady-

State Electromagnetic Scattering Problems Using the Time-Dependent Maxwell's Equations," *IEEE Trans. Microwave Theory Tech.*, **23**, 623 (1975).
Wait, J. R., "Excitation of an Enclosed Lossy Cylinder by an Aperature Source," *IEEE Trans. Microwave Theory Tech.*, **35**, 210 (1987).
Wei, C. K., H. T. Davis, E. A. Davis, and J. Gordon, "Heat and Mass Transfer in Water Laden Sandstone: Microwave Heating," *AIChE J.*, **31**, 842 (1985).
Welty, J. R., C. E. Wicks, and R. E. Wilson, *Fundamentals of Momentum, Heat and Mass Transfer*, 3rd ed., Wiley, New York (1984).
Yee, K. S., "Numerical Solution of Initial Boundary Value Problems Involving Maxwell's Equations in Isotropic Media," *IEEE Trans. Antennas Propagat.*, **14**, 302 (1966).

Manuscript received Dec. 9, 1991, and revision received June 10, 1992.